Journal of Materials Processing Tech. 286 (2020) 116814

Contents lists available at ScienceDirect

Journal of Materials Processing Tech.

journal homepage: www.elsevier.com/locate/jmatprotec

Two-phase viscoplastic model for the simulation of twin roll casting

Christian M.G. Rodrigues[a,*], Andreas Ludwig[a], Menghuai Wu[a], Abdellah Kharicha[a,b], Alexander Vakhrushev[b]

[a] Chair of Simulation and Modeling Metallurgical Processes, Metallurgy Department, Montanuniversitaet Leoben, Franz-Josef Street 18, 8700 Leoben, Austria
[b] Christian-Doppler Laboratory for Metallurgical Application of Magnetohydrodynamics, Montanuniversitaet of Leoben, Franz-Josef Street 18, 8700 Leoben, Austria

ARTICLE INFO

Associate Editor: S-J Na

Keywords:
Macrosegregation
Alloy solidification
Twin-roll casting
Computational modelling
Two-phase flow
Viscoplasticity

ABSTRACT

A two-phase Eulerian-Eulerian volume-averaged model was used to predict the outcome of the twin-roll casting process for inoculated Al-4 wt.% Cu alloys. The model is able to address the deformation of the mush during hot rolling by treating the solid/liquid mixture as a viscoplastic skeleton saturated with liquid. A parameter measuring the mean absolute deviation around the nominal composition was applied to the normalized macrosegregation distribution and the results were then used to determine an optimal process window where minimal compositional variation is achieved in the final strip. In the case of casting an 8 mm thick Al-4%Cu strip with rolls of 800 mm diameter, casting speeds between 40 and 42 mm/s and heat transfer rates given by HTCs between 5000 and 5250 W/m^2/K minimize the macrosegregation deviations in the strip and thus predict an optimal strip quality.

1. Introduction

The emergence of twin-roll casting has introduced a valid alternative for the production of light-weight metal strips at competitive costs for commercial applications. However, in order to increase the range of applicability of aluminum alloys and to become fully competitive with materials manufactured by conventional techniques in critical applications, further research needs to be undertaken so both physical and mechanical properties of the sheet maintain a certain level of quality while productivity is increased. In this respect, the role of modeling and simulation is critical to facilitate the interpretation of findings and to reduce costs normally associated with successive experimental trials.

Twin-roll casting is a complex technique that combines both metal casting and hot rolling in one single step. It is characterized by having a short solidification time and significant heat fluxes, which makes the procedure difficult to control and promotes the appearance of various defects. According to Yun et al. (2000), these include surface defects, internal defects and macroscopic buckling. Jin et al. (1982) and, later, Monaghan et al. (1993) observed in various experiments that the origin and severity of these defects can be directly connected to the operating conditions. Therefore, a proper understanding of the process, with a clear perception of the intricate dependencies between various operating parameters and the outcome, is decisive in controlling product quality.

Numerous mathematical models have been proposed in the literature to predict the fluid flow, heat transfer and solidification observed in twin-roll casters. For instance, Saxena and Sahai (2002) presented the results of a two-dimensional finite element based mathematical model of twin-roll casting. Lee et al. (2017) extended their approach to include mechanical analysis to the simulation, whereas Mortensen et al. (2015) introduced a Coulomb friction law to their model. Most of the models are based on single-phase finite element models with variable viscosity in the mushy zone. This approach has its merits but it fails to capture the interaction between the two phases present during the process, which is a significant aspect of the twin-roll casting process.

According to Nguyen et al. (1994), aluminum alloys in the semi-solid state have been found to behave like a solid skeleton saturated with interstitial liquid. Under this framework, solid and liquid become inherently coupled, which means that any motion of the skeleton affects directly the hydrodynamic response of the liquid flow. In a companion paper (Rodrigues et al., 2018), the relative motion between the two phases caused by the deformation of the mush in a twin-roll casting scenario was found to have a critical impact on the macrosegregation profile observed in the final metal strip. Under typical industrial operating conditions – where no liquid core prevails after passing the roll nip – the viscoplastic character of the semi-solid slurry must be taken into account when simulating such flows.

Since the early experimental observations of the influence of casting speed and heat transfer between the roll and the mush on the strip

* Corresponding author at: Franz-Josef-Str. 18, 8700 Leoben, Austria.
E-mail address: christian.gomes-rodrigues@unileoben.ac.at (C.M.G. Rodrigues).

https://doi.org/10.1016/j.jmatprotec.2020.116814
Received 5 February 2019; Received in revised form 4 May 2020; Accepted 29 June 2020
Available online 30 June 2020

quality reported by Lockyer et al. (1996), the interest on parameter studies that include these particular operating conditions has grown among the research community. In particular, numerical studies have been preferred as they have the advantage of reducing the experimental trial-and-error effort.

Saxena and Sahai (2002) presented the effect of the inlet velocity and strip/roll heat transfer coefficient (HTC) on the sump depth and strip exit temperature. They concluded that the strip exit temperature increases by increasing the inlet temperatures and the HTC, whereas the sump depth increases by increasing the inlet velocity and by decreasing the HTC. Interestingly, this study has the particularity of imposing a Dirichlet type boundary condition for the melt velocity at the inlet, as opposed to the more common approach of assuming a casting speed at the outlet (in combination with a velocity Neumann boundary condition at the inlet). Lee et al. (2017) also analyzed the effect of the HTC and the casting speed on the mechanical response between the solid strip and the moving rolls (referred as roll separation force). The authors found that casting speed has a greater effect on the roll separation forces than the HTC, and that both parameters have an inverse effect on the amount of solid fraction found under the roll (i.e., larger solid fractions are found with larger casting speeds but with smaller HTCs). Similar conclusions were also reported by Kim et al. (2010) and Sahoo et al. (2012) in computational studies carried out on high speed twin-roll casting.

The purpose of the work presented in this manuscript is to develop a comprehensive analysis of the effect of the casting speed and the roll surface to mush HTC on the strip properties in a two-phase model that takes into account the viscoplastic behavior of the mush. An optimal process window is also suggested for the present test case based on the conditions that produce minimal macrosegregation deviations.

2. Model description and simulation settings

2.1. Model in brief

The present model relies on a two-phase Euler-Euler volume-averaged model. It consists of the conservation equation of mass, momentum, species, and enthalpy, which are solved for each of the two phases (i.e., melt and equiaxed crystals) constituting the system. An additional transport equation for the grain number density is also taken into account. The conservation equations, source terms and auxiliary equations (as well as details on the discretization schemes) considered in the development of the model have been described in detail elsewhere (Rodrigues et al., 2019). For completeness, the equations used in the model are presented in Table 1 and are briefly described in the following.

A linearized binary Al-Cu phase diagram is considered, where the solute redistribution coefficient, k, and liquidus slope, m, are assumed to be constant. The liquid to solid mass transfer rate is estimated as function of the growth velocity of the equiaxed crystals, which in turn is governed by the concentration difference $c_l^* - c_l$. Liquid and solid interface concentrations c_l^* and c_s^*, respectively, can be obtained under the thermodynamic equilibrium concept assumed at the liquid-solid interface.

The present formulation regards the semi-solid slurry as a viscoplastic continuous solid skeleton saturated with interstitial liquid (Nguyen et al., 1994). The onset of the viscoplastic behavior corresponds to the volume fraction at which the crystals become able to sustain tensile loads. Drezet et al. (2014) referred to this threshold as the “rigidity point” and it is taken to occur at a critical solid fraction of $g_s^t = 0.57$. On the other hand, it is worth highlighting that the volume fraction at which the bridges between equiaxed crystals start to form but still no tensile loads can be sustained – generally identified as the coherency point – is not explicitly taken into account in the present formulation. However, it can still be recognized as the volume fraction at which the viscosity in the non-viscoplastic regime (given by Eq. 21) increases exponentially (which, for globular equiaxed crystals, is usually very close to the rigidity point).

The consideration of the viscoplastic material dynamics for higher solid fractions represents a distinctive feature of the model presented in this paper. Under this framework, the solid phase behaves as a continuous coherent structure with an apparent viscosity which depends on the equivalent strain rate tensor. In this regime, the solid skeleton is able to sustain significant tensile loads and the deformation and motion of the skeleton becomes then strictly connected to the hydrodynamic properties of the liquid flow. One can identify two main fluid flow regimes in this implementation: below the rigidity point the liquid is the dominating phase, which means that the solid motion is highly affected by the liquid, whereas, in the viscoplastic regime, the solid is the dominating phase and so the liquid motion is mainly governed by the dynamics of the solid phase. As it will be seen later, this comprehensive treatment of the flow behavior has been found very important in capturing the underlying physics of the process.

Equation 19 exhibits the distinctive characterization of the shear stress depending on the solid fraction. One can recognize immediately the presence of a second term in the viscoplastic regime. This can be referred to as a compression term and is critical in twin-roll casting simulations due to the hot rolling mechanism imposed during solidification. As for the viscosity, in the present work, the liquid viscosity is taken to be constant, whereas the solid viscosity depends on the solid fraction, as presented in Eq. 21.

The conservation equations presented in Table 1 are numerically implemented within the OpenFOAM software framework (version 5.0). The model here described can address solidification and transport of equiaxed crystals, as well as deformation and compression of the mush by considering a viscoplastic sub-model, whenever the solid fraction is above the rigidity point. Under this context, the twin-roll casting scenario is a great example where the applicability and robustness of the proposed algorithm can be tested.

2.2. Initial and boundary conditions

Fig. 1 shows the schematic diagram of the twin-roll casting process, as well as the regions where initial and boundary conditions were specified. The geometry replicates a typical twin-roll casting setup for the production of aluminum sheets, with the dimensions being shown in the diagram. Besides the inlet and outlet boundary conditions, the computational domain consists of three distinct sections (depicted in Fig. 1): the nozzle, the outer roll, and the strip. The boundary conditions used in the simulations are listed in Table 2.

Melt is injected at the inlet of the domain where a fixed pressure field is specified ($p = 10^5$ Pa). Dirichlet boundary conditions are imposed at the inlet to solid fraction ($g_s = 10^{-3}$, i.e., a practically zero amount), initial crystal diameter ($d = 5\,\mu\text{m}$), and liquid and solid species mass fractions ($c_\ell = 2.5\,\text{wt.\%}$ and $c_s = 0.36\,\text{wt.\%}$, according to the phase diagram). Heat flux boundary conditions are imposed to the roll and strip surfaces based on the reference sink temperature $T_\infty = 300\,\text{K}$ and the heat transfer coefficients (HTC) of $5500\,\text{W/m}^2/\text{K}$ for the roll section and $2\,\text{W/m}^2/\text{K}$ for the strip section. The remaining fields not given in Table 2 are set with homogeneous Neumann boundary conditions. The angular velocity of the rolls corresponds to the linear velocity specified at the outlet divided by the radius of the rolls.

The results have been obtained for an inoculated Al-4 wt.%Cu alloy ($\cong 2.5\,\text{wt.\%}$). The densities of the solid and liquid phases have been set as $2743\,\text{kg/m}^3$ and $2606\,\text{kg/m}^3$, respectively. In addition, the solid and liquid heat capacities have been defined as $c_{P,s} = 766\,\text{J/K}$ $\text{Cp}_s = 766\,\text{J/K}$ and $c_{P,\ell} = 1179\,\text{J/K}$, and the solid and liquid diffusion coefficients have been defined as $D_s^{Cu} = 8 \times 10^{-13}\,\text{m}^2/\text{s}$ and $D_l^{Cu} = 5 \times 10^{-9}\,\text{m}^2/\text{s}$.

Note that the density values for both solid and liquid phases as well as the HTC between the roll surfaces and the solid/liquid mixture have been assumed to be constant. The buoyancy effects have been found to

Table 1
Conservation equations, exchange terms, and auxiliary equations.

Conservations equations:		
Mass conservation:	$\frac{\partial g_i \rho_i}{\partial t} + \nabla \cdot (g_i \rho_i \mathbf{v}_i) = \mp M_{ls}$	(1)
Momentum conservation:	$\frac{\partial g_i \rho_i \mathbf{v}_i}{\partial t} + \nabla \cdot (g_i \rho_i \mathbf{v}_i \mathbf{v}_i) = -g_i \nabla p + \nabla \cdot g_i \boldsymbol{\tau}_i^{eff} \mp \mathbf{U}_{ls}$	(2)
Species conservation:	$\frac{\partial g_i \rho_i c_i}{\partial t} + \nabla \cdot (g_i \rho_i \mathbf{v}_i c_i) = \mp C_{ls}$	(3)
Enthalpy conservation:	$\frac{\partial g_i \rho_i h_i}{\partial t} + \nabla \cdot (g_i \rho_i \mathbf{v}_i h_i) = -\nabla \cdot \mathbf{q}_i \mp H_{ls}$	(4)
Grain transport:	$\frac{\partial n}{\partial t} + \nabla \cdot (\mathbf{v}_s n) = 0$	(5)
Exchange terms:		
Mass transfer:	$M_{\ell s} = v_r S_{\ell s} \rho_s \Phi_{\mathrm{imp}}$	(6)
Momentum transfer:	$\mathbf{U}_{\ell s} = \mathbf{U}_{\ell s}^d + \mathbf{U}_{\ell s}^p = K_{\ell s}(\mathbf{v}_\ell - \mathbf{v}_s) + u^* M_{\ell s}$	(7)
Species transfer:	$C_{\ell s} = k\, c_l^* M_{\ell s}, \quad where \;\; k = 0.145$	(8)
Enthalpy transfer:	$H_{ls} = h_c (T_\ell - T_s), \quad where \;\; h_c = 10^9 W\, m^{-2} K^{-1}$	(9)
Auxiliary equations:		
Crystal growth velocity	$v_r = \frac{D_l}{d_f/2(1 - d/d_f)} \frac{c_l^* - c_l}{c_l^*(1-k)}, \quad where \;\; D_l = 5 \times 10^{-9} m^2/s$	(10)
Crystal diameter	$d = 2 \times \sqrt[3]{\frac{g_s}{4/3\, \pi n}}$	(11)
Specific surface area	$S_{\ell s} = n \cdot \pi d^2$	(12)
Impingement factor	$\Phi_{\mathrm{imp}} = \min\left[g_l/(1 - \pi\sqrt{3}/8), 1\right]$	(13)
Interfacial liq. mass fraction	$c_l^* = (T - T_f)/m_{ls}, \quad with \;\; T_f = 933.5\, K \;\; and \;\; m_{ls} = -344\, K$	(14)
Drag coefficient	$K_{ls} = \begin{cases} 18 g_l^2 \frac{\mu_l g_s C_\varepsilon}{d^2} \text{for } g_s < g_s^t & with \;\; C_\varepsilon = 10 g_s \big/ g_l^3 \\ g_l^2 \frac{\mu_l}{K} \text{ for } g_s \geq g_s^t & with \;\; K = \frac{d^2}{180} g_l^3 \big/ g_s^2 \end{cases}$ $where \;\; g_s^t = 0.57$	(15)
Average velocity	$u^* = \begin{cases} \mathbf{v}_l \textit{during solidification} \\ \mathbf{v}_s \textit{during melting} \end{cases}$	(16)
Heat flux:	$\mathbf{q}_i = \alpha_i \nabla h_i, \quad where \;\; \alpha_l = 0.065\, kg/m\, s \;\; and \;\; \alpha_s = 0.2\, kg/m\, s$	(17)
Shear stress treatment:		
Liquid shear stress	$\boldsymbol{\tau}_l^{eff} = \boldsymbol{\tau}_\ell = 2\mu_\ell \mathrm{dev}(\dot{\boldsymbol{\varepsilon}}_\ell) where \;\; \dot{\boldsymbol{\varepsilon}}_l = 1/2(\nabla \mathbf{v}_l + (\nabla \mathbf{v}_l)^T)$	(18)
Solid shear stress	$\boldsymbol{\tau}_s^{eff} = \begin{cases} 2\mu_s \mathrm{dev}(\dot{\boldsymbol{\varepsilon}}_s) & \text{for} g_s \leq g_s^t \\ 2\frac{\mu_s^{\mathrm{app}}}{A} \mathrm{dev}(\dot{\boldsymbol{\varepsilon}}_s) + \mu_s^{\mathrm{app}} \left(\frac{1}{9B}\right) \mathrm{tr}(\dot{\boldsymbol{\varepsilon}}_s) \mathbf{I} & \text{for} g_s > g_s^t \end{cases}$ $where \;\; \dot{\boldsymbol{\varepsilon}}_s = 1/2(\nabla \mathbf{v}_s + (\nabla \mathbf{v}_s)^T), \quad A = 3/g_s^{6.47} \;\; and \;\; B = 0.009(1/g_s^{6.94} - 1)$	(19)
Liquid viscosity	$\mu_\ell = 0.013\, \mathrm{Pa \cdot s}$	(20)
Solid viscosity	$\mu_s^{eff} = \begin{cases} \frac{\mu_\ell}{g_s}\left(\left(1 - \frac{g_s}{g_s^p}\right)^{-2.5 g_s^p} - (1 - g_s)\right) & \text{for} g_s \leq g_s^t \\ 3K_v (\sqrt{3}\, \dot{\varepsilon}_s^{\mathrm{eq}})^{m-1} & \text{for} g_s > g_s^t \end{cases}$ $where \;\; g_s^p = 0.585, \quad K_v = 6.31 \times 10^6 Pa.\, s, \quad m = 0.213$ $and \;\; \dot{\varepsilon}_s^{\mathrm{eq}} = \sqrt{\frac{2}{A}(\dot{\boldsymbol{\varepsilon}}_s : \dot{\boldsymbol{\varepsilon}}_s) - \left(\frac{2}{3A} - \frac{1}{9B}\right) \mathrm{tr}(\dot{\boldsymbol{\varepsilon}}_s)^2}$	(21)

Note that the flow is assumed to be laminar in the present model. Considering that the characteristic size L (casting size) in the domain is assumed to be 0.008 m, and the corresponding reference liquid velocity is around 0.04 m/s, the system Reynolds number ($\mathrm{Re} = L\, \mathbf{v}_l\, \rho_l / \mu_l$) becomes equal to about 64.2, which is less than the critical number 2100 for the onset of turbulence flow.

have no significant influence on the observed simulation results, as the process is mainly driven by the rolling mechanisms. Therefore, the effect of gravity is neglected in the present work.

Since the width of the sheet is in concept much larger than its thickness, the test case is considered to be 2D. A structured mesh composed of 5700 quadrilateral cells was used, which corresponds to an average cell size of approximately 0.85 mm per 0.47 mm. The same number of cells along vertical axis was used at inlet and outlet, and so inherently a more refined mesh ensues as the domain becomes

Table 2
Boundary conditions for velocity and temperature fields.

	solid velocity	liquid velocity	enthalpy/temperature
Inlet	pressure inlet	pressure inlet	925 K
Nozzle	free-slip	no slip	925 K
Roll	free-slip	no slip (0.1 rad/s)	heat flux (HTC = 5500W/m^2/K)
Strip	free-slip	no slip (0.040 m/s)	heat flux (HTC = 2 W/m^2/K)
Outlet	0.040 m/s	0.040 m/s	zero gradient

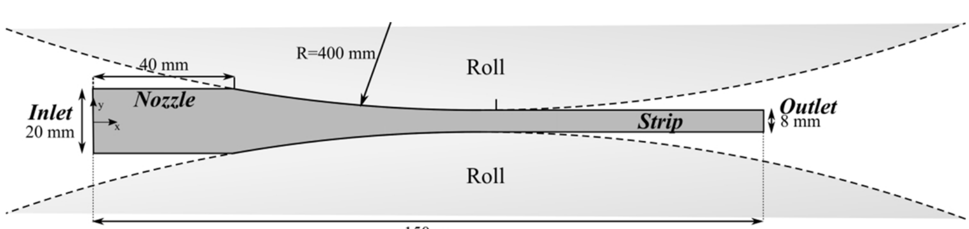

Fig. 1. Schematic representation of the twin-roll continuous casting process (retrieved from Rodrigues et al., 2019).

narrower. The time step was variable to maintain the convergence and stability of the numerical procedure, but remained in the order of 10^{-4} s a few moments after the start of the simulation. A typical run of the simulation takes around 5 h to reach steady-state on an Intel ® Core ™ i7 − 6700 local workstation using a single core.

The twin-roll casting operating conditions are critical to avoid internal defects and improve the quality of the cast strips. Macrosegregation is caused by a relative motion between the solute-depleted solid and solute-enriched melt and so relevant compositional variations can be detrimental to mechanical performance due to the variation in the mechanical properties throughout the cast product. In the present work, the prediction results are presented in terms of normalized macrosegregation ($c_{mix}/c_0 - 1$), with the initial alloy composition being given by the value 0, whereas positive or negative macrosegregation are illustrated with positive or negative values, respectively.

Although the computational model employed in the present work is the same as the one used in a companion paper (Rodrigues et al., 2019), the boundary conditions are slightly different (i.e., the HTC enforced in the strip section is much lower) and, more importantly, the objectives set in each work are different. In Rodrigues et al. (2019), the analysis of the macrosegregation distribution in a twin roll casting scenario along with the corresponding description of the relative flow between the phases (that leads to the macrosegregation formations) has been reported. Here, the analysis is limited to the quantitative understanding of how operating conditions such as casting speed and heat transfer coefficient between roll surface and mush affect the final outcome.

3. Results

3.1. Operation range of interest

The rigid shell is defined as the material with a solid fraction above 57 %. Fig. 2 shows the direct dependence between casting speed and rigid shell thickness. It demonstrates that an increase in casting speed leads to a decrease in the expected viscoplastic shell thickness at the roll nip. This can be explained by the fact that with a faster rotation of the cooling rolls, there is less time for heat extraction which makes the solidification process less effective.

Above 42 mm/s of casting speed (and for HTC = 5500 W/m^2/s), the size of each of the viscoplastic shells at the roll nip becomes smaller than half the thickness of the final strip (identified in the plot with the dashed line). As the heat transfer after having passed the roll nip decreases by three orders of magnitude, solidification slows down drastically and in consequence the solid fraction in the strip center might never reach the rigidity limit and the strip might thus split into two parts. To obtain a fully viscoplastic and thus a stable strip at the toll nip even for casting speeds at and above 42 mm/s, the heat transfer between strip and rolls must be enlarged and thus the casting pressure must be increased. This will be discussed later in details.

At the other end of the spectrum established in Fig. 2 lies the casting

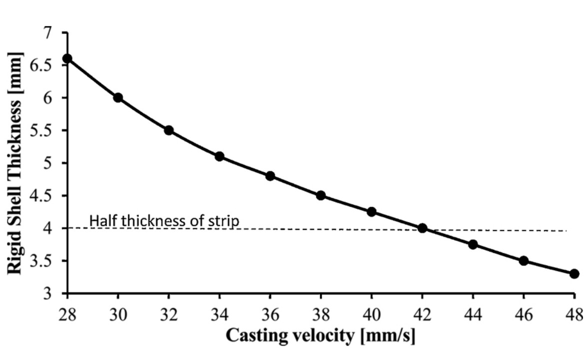

Fig. 2. Rigid shell thickness prediction as a function of casting speed.

speed of 28 mm/s. In this case, the velocity is such that it gives rise to thicker semi-solid shells developing on the roll surfaces, and consequently, there is a large quantity of mush that has to be compressed in the region where the two rigid shells merge together. As a result, material is squeezed out of the mush against casting direction, giving rise to a backward flow along the central plane of the domain. This causes both segregated melt and solid crystals to be transported from a cold to a hot region, eventually changing their composition and inducing melting to occur in this particular area. Such description can be easily recognized in Fig. 3, with the melting region being identifiable by the dark blue color along the centerline of the domain upstream of the kissing point. The term "kissing point" has been adopted in the present manuscript to identify the upstream-most location along the centerline of the domain where merging between the two rigid shells initiates.

Liquid being squeezed back against casting directions (towards the sump) was already reported in the experimental studies of Lockyer et al. (1996) due to the deformation of the semi-solid. Such an occurrence was associated with the appearance of defects in the central plane of the sheet. To our knowledge, this channel formation has never been reported in other numerical works. This highlights the capabilities of the current model in handling complex situations, such as the one reported here where the relative velocity between the phases must be accurately predicted for a physically sound description of the twin-roll casting process.

The distance between the nozzle and the kissing point is defined as the sump depth. It is very often used as an indicator of the severity of potential defects. It is commonly accepted that the minimization of the sump depth is key in improving the quality of the cast strips. Both the depth and shape of the sump are greatly sensitive to the process variables like casting speed and heat transfer coefficient. In the present section, the simulation results for different casting speeds and heat transfer coefficients are presented. Table 3 summarizes the series of simulations performed in this work.

3.2. Effect of casting speed

Fig. 4 illustrates the steady-state results of solid fraction (top half) and temperature (bottom half) for an HTC between the rolls and the solid/liquid mixture of 5500 W/m^2/K and casting speeds between 36 mm/s and 48 mm/s. The solid fraction distribution at the outlet (approximately similar as at the roll nip) depicts the solidification level reached at the end of the casting process. After the melt reaches the region between the two water-cooled counter-rotating rolls, it starts to solidify. As a result, a viscoplastic shell develops on each of the moving roll surfaces, which grows towards the centerline of the domain and eventually merge into one continuous single strip.

How much hot rolling is enforced during the twin-roll casting process depends on how far from the roll nip is the sump depth. As described above, as the sump depth gets farther away from the roll nip, the mush becomes subjected to more hot rolling, and correspondingly, to more compression forces. This is illustrated in Fig. 5, where the steady-state results of the equivalent stress (top half) and the solid effective viscosity (bottom half) for casting speeds of 36 mm/s, 40 mm/s, 44 mm/s, and 48 mm/s are presented.

The need for consistent production of high-quality strips makes it imperative to develop a quantitative understanding of the operating conditions that lead to that outcome. As referred before, the macrosegregation results have been used here as an indication of the quality of the strip. Large compositional variations indicate that the relative motion between the two phases is particularly significant, and this can have a detrimental impact on the processing behavior of the alloy. In the present work, the mean absolute deviation of the macrosegregation formations has been employed to measure such statistical dispersion and is plotted in Fig.6.

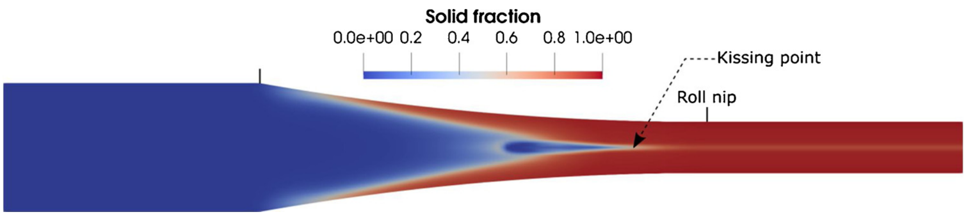

Fig. 3. Steady-state solid fraction distribution in case with low casting speed (28 mm/s).

Table 3
Series of simulations performed.

	Simulation series 1	Simulation series 2
Fixed parameter	Heat transfer coefficient HTC = 5500 W/m^2/K	Casting speed $\mathbf{v}_i^{cast} = 40$ mm/s
Studied parameter	$\mathbf{v}_i^{cast} = 36$ mm/s	HTC = 4500 W/m^2/K
	$\mathbf{v}_i^{cast} = 40$ mm/s	HTC = 5000 W/m^2/K
	$\mathbf{v}_i^{cast} = 44$ mm/s	HTC = 5500 W/m^2/K
	$\mathbf{v}_i^{cast} = 48$ mm/s	HTC = 6000 W/m^2/K

3.3. Effect of heat transfer coefficient

The second parameter that has been analyzed in this study is the HTC between the roll surfaces and the solid/liquid mixture.

Steady-state results of solid fraction (top half) and liquid temperature (bottom half) for HTCs between 4500 W/m^2/K and 6000 W/m^2/K at a casting speed of 40 mm/s are presented in Fig. 7. Note that below 4500 W/m^2/K, the cooling rate was not high enough for the two rigid shells to meet at the kissing point, whereas above 6000 W/m^2/K, the compression forces were such that it would give rise to a backward flow similar to the outcome reported in Fig. 3. As a result, these cases were not considered in the following analysis.

Contrary to the trend observed with the increase in the casting speed, the increase in HTC values results in an increase in heat loss from the mush to the rolls, which leads to an increase in the thickness of the rigid shell and a decrease in the sump depth. Also, the kissing point between the two rigid shells takes place more and more upstream, and thus increasingly stronger rolling effects are to be expected as the HTC values increase. These findings are corroborated by the quantitative results shown in Fig. 8, where the equivalent stresses predicted are plotted along two longitudinal axes for the different HTCs evaluated.

Fig. 9 illustrates the mean absolute deviation around the nominal composition of the normalized macrosegregation results as a function of the different HTCs studied. The data has been considered along the cross-section of the strip near the outlet plane.

4. Discussion

4.1. Effect of casting speed

In Fig. 4, it can be seen that as the casting speed increases, the depth of the sump region increases. Such finding is in line with observations reported by Lockyer et al. (1996). This is because the heat loss through the cooling rolls decreases as demonstrated in the bottom half of Fig. 4,

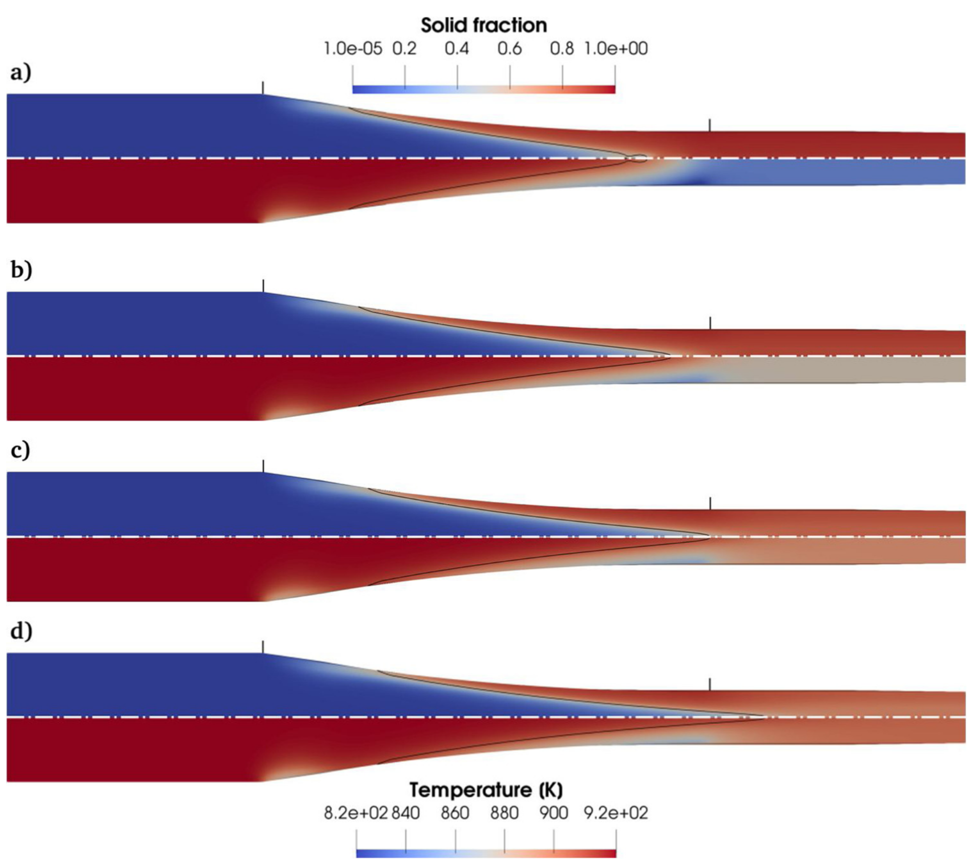

Fig. 4. Steady-state results of solid fraction (top half) and liquid temperature (bottom half) for casting speeds of a) 36 mm/s, b) 40 mm/s, c) 44 mm/s, and d) 48 mm/s.

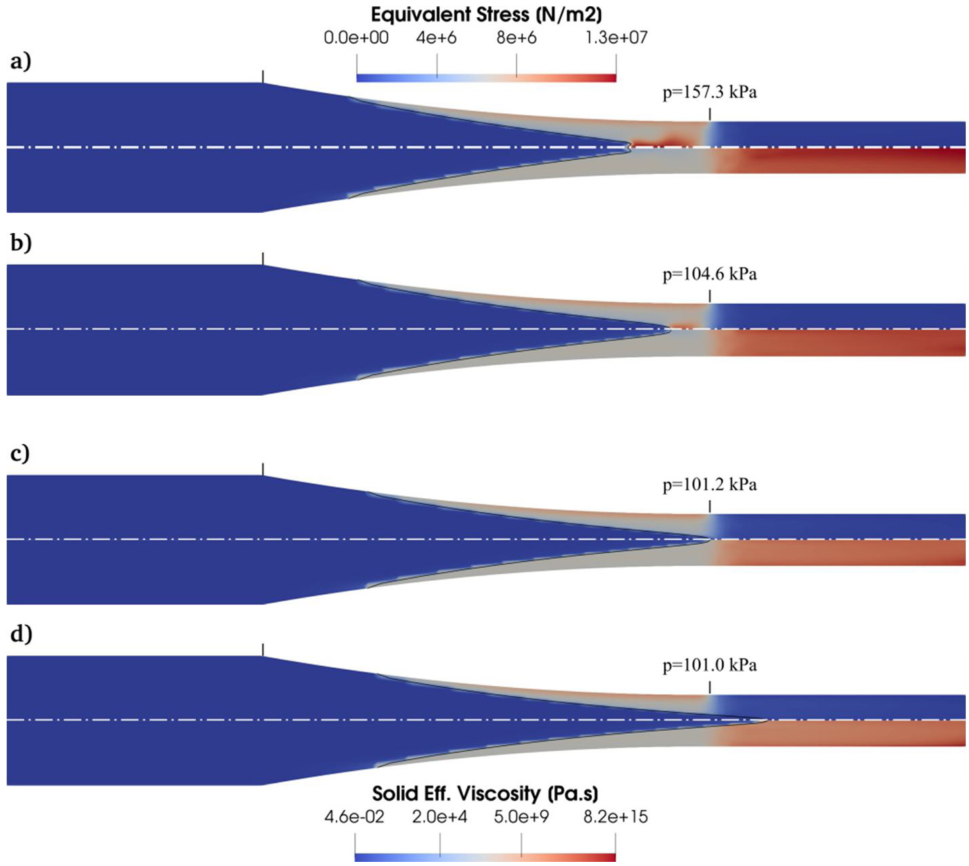

Fig. 5. Steady-state results of the equivalent stress (top half) and solid effective viscosity (bottom half) for casting speeds of a) 36 mm/s, b) 40 mm/s, c) 44 mm/s, and d) 48 mm/s. Solid effective viscosity (bottom half) is shown with logarithmic scale. Rolling pressure at the roll nip is specified in each case.

where the temperature distribution is shown. As a result, increasingly thinner rigid shells form on the roll surfaces, which take longer to meet each other at the centerline of the domain. Such conditions are known to be related to lower stress forces near the kissing point, as shown in Fig. 5. Similarly, notice the decrease in the rolling pressure at the roll nip (specified at the second marker) as the casting speed increases.

It is worth mentioning that the equivalent stress illustrated in Fig. 5 corresponds to an expression used specifically in the viscoplastic regime (and thus it is shown to be zero for solid fractions below the rigidity point). It has been proposed by Nguyen et al. (1994) as a measure of the stress field in a semi-solid system when subjected to compression forces. This obviously accounts for both the solid phase deformation and the liquid flow induced by the solid skeleton deformation. The equivalent stress equation can be written as follows:

$$\sigma_s^{eq} = \sqrt{3}K_v(\sqrt{3}\dot{\varepsilon}_s^{\mathrm{eq}}) \tag{22}$$

where the viscoplastic consistency, K_v, and the strain-rate sensitivity, m, are defined in Table 1.

Besides the region near the roll surfaces where the deformation of the mush leads to an increase in the stress tensor, very high stresses can also be found around the kissing point in the cases with lower casting speeds (i.e., Fig.5 a and b). This is due to the compression forces that develop when solidification is mostly completed before reaching the roll nip. This is typically referred to as hot rolling. On the other hand, as

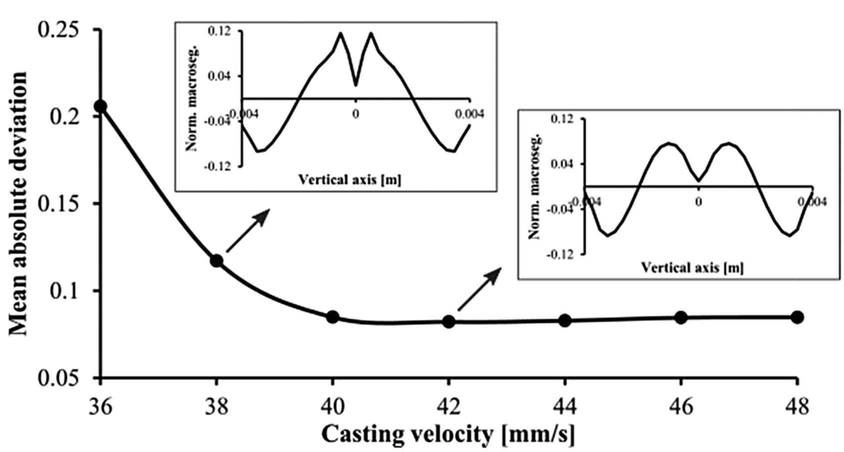

Fig. 6. Mean absolute deviation around nominal composition of normalized macrosegregation as a function of casting velocity. Normalized macrosegregation along vertical axis for simulation with casting velocities of 38 and 42 mm/s are presented.

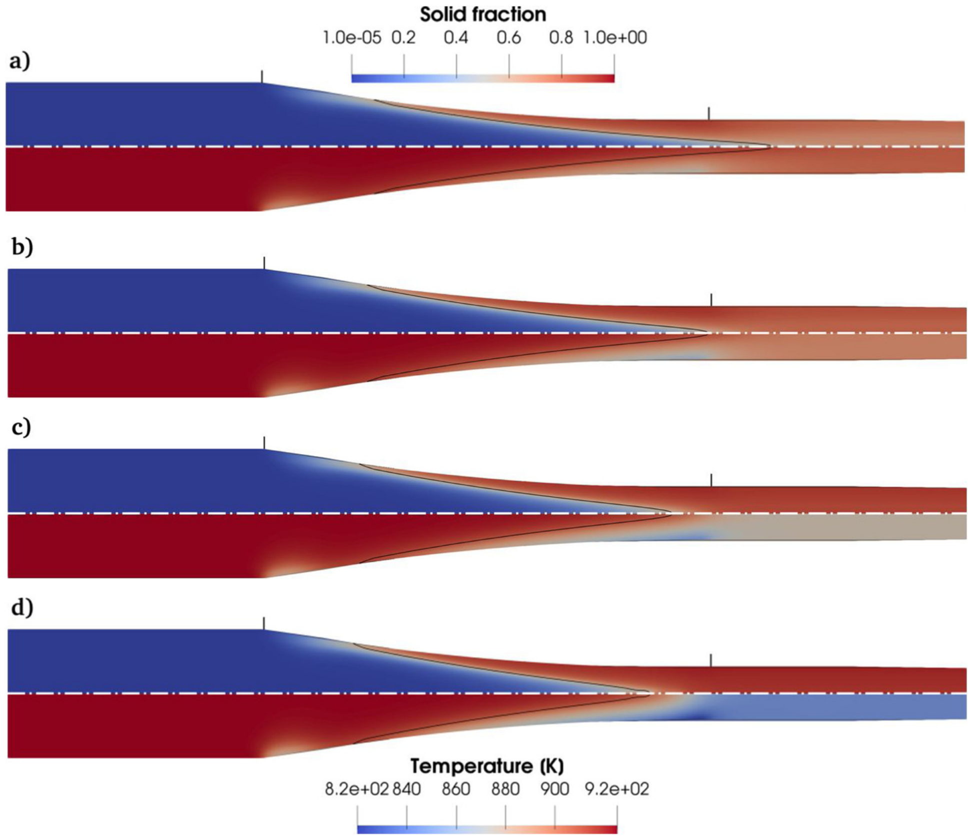

Fig. 7. Steady-state results of solid fraction (top half) and liquid temperature (bottom half) for HTCs of a) 4500 W/m^2/K, b) 5000 W/m^2/K, c) 5500 W/m^2/K, and d) 6000 W/m^2/K.

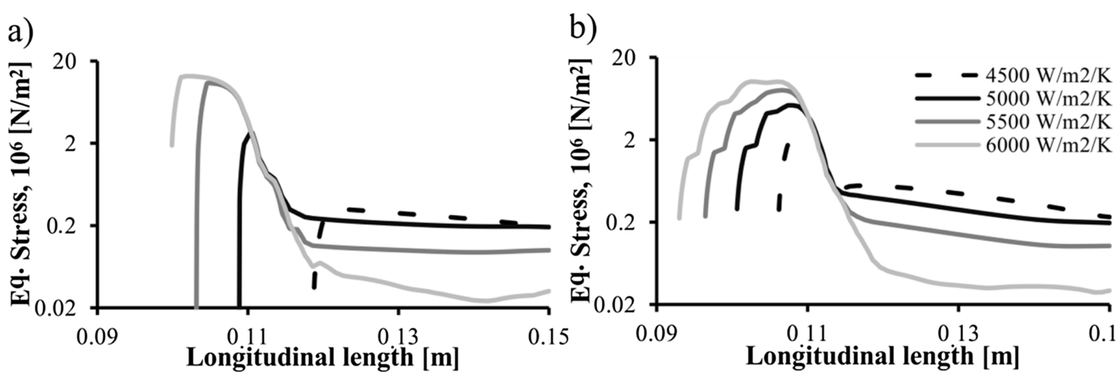

Fig. 8. Quantitative results of the equivalent stress along longitudinal axis at a) y = 0.000 m and b) y = 0.001 m. Vertical axis has a logarithmic scale.

the velocity increases, the two rigid shells only fully merge after the roll nip is reached. As there is still a layer of liquid present between the rigid shells while they are subjected to compression, no significant stresses are observed in these cases.

Another interesting finding detectable in Fig. 5 is the sudden decrease in the equivalent stress in the last section of the domain. As reported above, the roll nip identifies the point in the domain where the boundary surfaces become horizontal. This means that no relative flow is expected purely from the physical constraints of the domain under consideration. As a result, the macroscopic velocity gradients in the solid in this region become very small which means that, according to Eq. 22, the equivalent stress in the strip section also decreases by several orders of magnitude, as observed in Fig. 5.

As for the effective solid viscosity, it jumps several orders of magnitude once the solid/liquid mixture is treated as a viscoplastic skeleton saturated with liquid. This results in a stiff structure that is expected to move as a whole with casting speed. Furthermore, one can notice that there is an inverse trend between the viscosity distributions presented in the bottom half of Fig. 5 and the equivalent stress depicted on the top part. This relation can be identified by combining Eq. 21 and Eq. 22. This also explains why the apparent solid viscosity jumps again several orders of magnitude at the roll nip (i.e., when the equivalent strain rate and the equivalent stress in the solid phase reach very low values).

The mean absolute deviation of the macrosegregation formations is introduced in Fig. 6 as a measure of statistical dispersion around a reference value. The parameter is obtained by identifying the maximum and minimum values of the normalized macrosegregation results along the cross-section of the strip near the outlet, and then calculating the mean absolute deviation around the nominal composition based on the data gathered. The idea is to determine how far the values are spread around the nominal composition of the normalized macrosegregation results and use it as an indication of the product quality. Accordingly, a

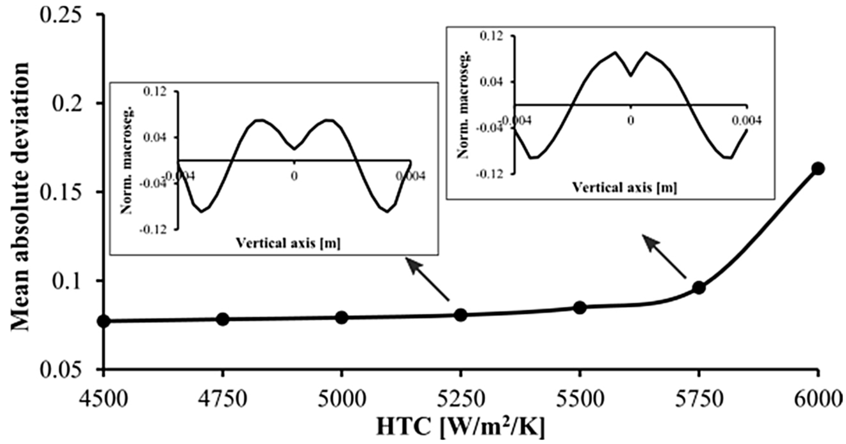

Fig. 9. Mean absolute deviation around nominal composition of normalized macrosegregation as a function of HTC. Normalized macrosegregation along vertical axis for simulation with HTCs of 5250 and 5750 W/m^2/K are presented.

test case with a large mean absolute deviation value implies that the quality of the final strip is lower than a corresponding test case with a lower mean absolute deviation because the larger spread between the positive and negative macrosegregation predictions indicates a more significant relative flow.

From Fig. 6, one can observe that as the velocity of the rolls increases, the mean absolute deviation parameter decreases abruptly first, reaches a local minimum at a casting speed between 40 mm/s and 42 mm/s, and then starts to increase very slightly again from that point on. According to the data presented, the optimal process window for the twin-roll casting scenario discussed in this paper should be defined with a casting speed between 40 mm/s and 42 mm/s for minimal deviations in the macrosegregation results.

Roll velocities above 42 mm/s produce only a slight increase in the mean absolute deviation values, as shown in Fig. 6. However, it is important to keep in mind that, as the velocity increases, Lee et al. (2015) found that the chance for insufficient solidification also increases, which has an impact on the strip quality.

4.2. Effect of heat transfer coefficient

The heat transfer achieved during the twin-roll casting process is a complex mechanism that changes throughout the roll bite. Several studies have reported that the heat transfer coefficient is influenced by a number of operating conditions, such as superheat (Coates and Argyropoulos, 2007), casting size, surface roughness (Wang and Matthys, 2002) and surface coating (Muojekwu et al., 1995).

Due to the difficulty in obtaining accurate heat flux measurements, the data are usually employed as a guide in solidification modeling. Here, constant HTCs have been considered in the simulations. The different outcomes obtained by varying the HTC values should provide some insight into the optimal range within which cast products with lower macrosegregation deviations can be obtained.

Fig. 8 plots the quantitative results of the equivalent stress along two longitudinal axes. Along the centerline, the increase in the HTC values leads to an increase in the maximum equivalent stresses, which in turn corresponds to the location where the two rigid shells merge in each case. Downstream of this point, the stresses tend to decrease until a roughly constant value is achieved. Interestingly, in the cases with higher compression forces, because of the flow dynamics that are still present after the hot rolling is finished (due to the propagation of the relative flow towards the strip section that was mentioned before), the coherent structure ends up by achieving a more balanced arrangement, with lower equivalent stresses.

The comparison of the two higher HTC cases shows that along the centerline the maximum equivalent stress obtained does not differ considerably, whereas in the cases with lower HTC values the difference is more substantial. However, if the analysis is performed slightly off centerline values (i.e., along the longitudinal axis located at $y = 0.001$ m), the difference between each case is more uniform, as illustrated in Fig. 8 b). Since the transition towards the viscoplastic regime is smoother, the equivalent stress profile appears to be more homogeneous across the different cases. This illustrates the importance of proper evaluation of the data considered.

It can be seen in Fig. 9 that HTC has a strong influence on the macrosegregation distribution, particularly for higher values. The results show that as the HTC values increase, the solidification rate also increases, which then leads to higher levels of hot rolling between the kissing point and the roll nip, and thus larger deviations from nominal composition of the alloy.

On the other hand, even though the mean absolute deviation in the case with HTC = 4500 W/m^2/K is the lowest, the sump depth exceeds the roll nip and this exposes the procedure to potentially incomplete solidification. According to Lee et al. (2015), incomplete solidification increases the possibility of failure of the process, although the measured compression force in their experiments was found to be low.

This leaves the range between 4750 W/m^2/K and 5250 W/m^2/K where the slope of the mean absolute deviation is almost negligible. However, it is important to remember that the present results have been obtained for a casting speed of 40 mm/s. One might be tempted to increase the production rate – while still performing within the optimal window range defined previously – and thus increase the casting speed to 42 mm/s. Under these conditions, the HTC would have to increase accordingly to a minimum value of 5000 W/m^2/K in order to avoid incomplete solidification at the end of the process. Therefore, for the scenario under analysis, the optimal window for best cast products would be defined by HTCs between 5000 W/m^2/K and 5250 W/m^2/K.

5. Conclusion

The successful production of defect-free strips during twin-roll casting requires strict control of the operating conditions involved in the process, as well as a good understanding of how the interaction between them affects the results. Proper optimization of these parameters can lead to significant improvements in the pursuit of defect free products. Therefore, the influence of casting speed and heat transfer coefficient on the results has been studied. A quantitative parameter has been employed to measure the macrosegregation dispersion and assess the quality of the cast products in terms of compositional variations. The following conclusions can be drawn:

- There is a very specific range of casting speeds where acceptable results are obtained. Too low roll velocity leads to excessive hot rolling (which induces squeezing out of material against casting direction), whereas too high roll velocity does not allow the two rigid shells to merge before the roll nip is reached which can lead to problems related to insufficient solidification.

- The heat transfer considered in the simulations is an effective representation of the cooling rates found in casting. Similarly to the casting speed, proper results are only obtained within a very narrow range of HTC outside of which incomplete solidification or excessive hot rolling appears.
- A narrow process window has been suggested where the production of thin strips by twin-roll casting finds favorable conditions to achieve products with lower macrosegregation deviations. For the 8 mm thick Al-4%Cu strip being produced with rolls of 800 mm diameter, casting speeds between 40 mm/s and 42 mm/s and HTCs between 5000 $W/m^2/K$ and 5250 $W/m^2/K$ define the optimal process window.

CRediT authorship contribution statement

Christian M.G. Rodrigues: Investigation, Software, Methodology, Conceptualization, Writing - original draft. **Andreas Ludwig:** Investigation, Funding acquisition, Project administration, Supervision, Writing - review & editing. **Menghuai Wu:** Investigation, Writing - review & editing. **Abdellah Kharicha:** Investigation, Writing - review & editing. **Alexander Vakhrushev:** Software, Writing - review & editing.

Declaration of Competing Interest

The authors declare that they have no known competing financial interests or personal relationships that could have appeared to influence the work reported in this paper.

Acknowledgments

This work was financially supported by the FWF Austrian Science Fund (P28785-N34) which the authors gratefully acknowledge. The authors acknowledge the financial support by the Austrian Federal Ministry of Economy, Family and Youth and the National Foundation for Research, Technology, and Development within the framework of the Christian Doppler Laboratory for Metallurgical applications of Magneto-hydrodynamics.

References

Coates, B., Argyropoulos, S.A., 2007. The effects of surface roughness and metal temperature on the heat-transfer coefficient at the metal mold interface. Metall. Mater. Trans. B Process Metall. Mater. Process. Sci. 38, 243–255. https://doi.org/10.1007/s11663-007-9020-y.

Drezet, J., Mireux, B., Szaraz, Z., Pirling, T., 2014. Determination of coherency and rigidity temperatures in Al-Cu alloys using in situ neutron diffraction during casting. Miner. Met. Mater. Soc. 66, 1425–1430. https://doi.org/10.1007/s11837-014-1018-8.

Jin, I., Morris, L.R., Hunt, J.D., 1982. Centerline segregation. J. Met. 70–75.

Kim, M.-S., Arai, Y., Hori, Y., Kumai, S., 2010. Formation of internal crack in high-speed twin-roll cast 6022 aluminum alloy strip. Mater. Trans. 51, 1854–1860. https://doi.org/10.2320/matertrans.L-M2010818.

Lee, Y.S., Kim, H.W., Cho, J.H., 2015. Process parameters and roll separation force in horizontal twin rollcasting of aluminum alloys. J. Mater. Process. Technol. 218, 48–56. https://doi.org/10.1016/j.jmatprotec.2014.11.031.

Lee, Y.S., Kim, H.W., Cho, J.H., Chun, S.H., 2017. Coupled thermal-fluid-mechanics analysis of twin roll casting of A7075 aluminum alloy. Met. Mater. Int. 23, 923–929. https://doi.org/10.1007/s12540-017-6275-y.

Lockyer, S.A., Yun, M., Hunt, J.D., Edmonds, D.V., 1996. Micro- and macrodefects in thin sheet twin-roll cast aluminum alloys. Mater. Charact. 37, 301–310. https://doi.org/10.1016/S1044-5803(97)80019-8.

Monaghan, D.J., Henderson, M.B., Hunt, J.D., Edmonds, D.V., 1993. Microstructural defects in high productivity twin-roll casting of aluminium. Mater. Sci. Eng. A 173, 251–254. https://doi.org/10.1016/0921-5093(93)90224-3.

Mortensen, D., Fjaer, H.G., Lindholm, D., Karhausen, K.F., Kvalevag, J.S., 2015. Modelling of the twin roll casting process including friction. Light Metals 2015, 1241–1247. https://doi.org/10.1002/9781119093435.ch208.

Muojekwu, C.A., Samarasekera, I.V., Brimacombe, J.K., 1995. Heat transfer and microstructure during the early stages of metal solidification. Metall. Mater. Trans. B 26B, 361–382.

Nguyen, T.G., Favier, D., Suery, M., 1994. Theoretical and experimental study of the isothermal mechanical behaviour of alloys in the semi-solid state. Int. J. Plast. 10, 663–693.

Rodrigues, C.M.G., Ludwig, A., Kharicha, A., Wu, M., 2018. Modeling of the twin-roll casting process: transition from casting to rolling. Trans. Indian Inst. Met. https://doi.org/10.1007/s12666-018-1423-8.

Rodrigues, C.M.G., Ludwig, A., Kharicha, A., Wu, M., Vakhrushev, A., 2019. A comprehensive analysis of macrosegregation formation during twin-roll casting. Asymmetric Transf. Hydrog. C = n Bond. With Met. Catal. 50, 1334–1350. https://doi.org/10.1007/s11663-019-01527-x.

Sahoo, S., Kumar, A., Dhindaw, B.K., Ghosh, S., 2012. Modeling and experimental validation of rapid cooling and solidification during high-speed twin-roll strip casting of Al-33 wt pct Cu. Asymmetric Transf. Hydrog. C = n Bond. With Met. Catal. 43, 915–924. https://doi.org/10.1007/s11663-012-9659-x.

Saxena, A., Sahai, Y., 2002. Modeling of fluid flow and heat transfer in twin-roll casting of aluminum alloys. Mater. Trans. 43, 206–213. https://doi.org/10.2320/matertrans.43.206.

Wang, G.X., Matthys, E.F., 2002. Experimental determination of the interfacial heat transfer during cooling and solidification of molten metal droplets impacting on a metallic substrate: effect of roughness and superheat. Int. J. Heat Mass Transf. 45, 4967–4981. https://doi.org/10.1016/S0017-9310(02)00199-0.

Yun, M., Lokyer, S., Hunt, J.D., 2000. Twin roll casting of aluminium alloys. Mater. Sci. Eng. A 280, 116–123. https://doi.org/10.1016/S0921-5093(99)00676-0.